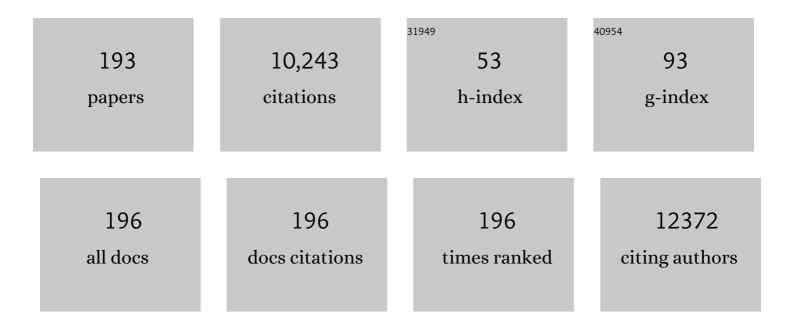
Jun-Ying Zhang

List of Publications by Year in descending order

Source: https://exaly.com/author-pdf/4722754/publications.pdf Version: 2024-02-01



#	Article	IF	CITATIONS
1	Metal-Free Photocatalyst for H ₂ Evolution in Visible to Near-Infrared Region: Black Phosphorus/Graphitic Carbon Nitride. Journal of the American Chemical Society, 2017, 139, 13234-13242.	6.6	907
2	Doping-Enhanced Short-Range Order of Perovskite Nanocrystals for Near-Unity Violet Luminescence Quantum Yield. Journal of the American Chemical Society, 2018, 140, 9942-9951.	6.6	548
3	Structural and Optical Properties of Uniform ZnO Nanosheets. Advanced Materials, 2005, 17, 586-590.	11.1	313
4	Photocatalytic properties of BiOX (X = Cl, Br, and I). Rare Metals, 2008, 27, 243-250.	3.6	297
5	Au/La ₂ Ti ₂ O ₇ Nanostructures Sensitized with Black Phosphorus for Plasmonâ€Enhanced Photocatalytic Hydrogen Production in Visible and Nearâ€Infrared Light. Angewandte Chemie - International Edition, 2017, 56, 2064-2068.	7.2	284
6	Teâ€Doped Black Phosphorus Fieldâ€Effect Transistors. Advanced Materials, 2016, 28, 9408-9415.	11.1	241
7	Preparation of a new long afterglow blue-emitting Sr2MgSi2O7-based photoluminescent phosphor. Journal of Materials Science Letters, 2001, 20, 1505-1506.	0.5	235
8	Protruding Pt single-sites on hexagonal ZnIn2S4 to accelerate photocatalytic hydrogen evolution. Nature Communications, 2022, 13, 1287.	5.8	198
9	Effects of Defects on Photocatalytic Activity of Hydrogen-Treated Titanium Oxide Nanobelts. ACS Catalysis, 2017, 7, 1742-1748.	5.5	173
10	The characterization and mechanism of long afterglow in alkaline earth aluminates phosphors co-doped by Eu2O3 and Dy2O3. Materials Chemistry and Physics, 2001, 70, 156-159.	2.0	165
11	X-ray-activated long persistent phosphors featuring strong UVC afterglow emissions. Light: Science and Applications, 2018, 7, 88.	7.7	159
12	Defect Engineering of Air-Treated WO ₃ and Its Enhanced Visible-Light-Driven Photocatalytic and Electrochemical Performance. Journal of Physical Chemistry C, 2016, 120, 9750-9763.	1.5	147
13	Cs ₄ PbBr ₆ /CsPbBr ₃ Perovskite Composites with Near-Unity Luminescence Quantum Yield: Large-Scale Synthesis, Luminescence and Formation Mechanism, and White Light-Emitting Diode Application. ACS Applied Materials & Interfaces, 2018, 10, 15905-15912.	4.0	135
14	Ultrathin ZnIn2S4 nanosheets with active (110) facet exposure and efficient charge separation for cocatalyst free photocatalytic hydrogen evolution. Applied Catalysis B: Environmental, 2020, 265, 118616.	10.8	132
15	Ultrafast Charge Separation for Full Solar Spectrum-Activated Photocatalytic H ₂ Generation in a Black Phosphorus–Au–CdS Heterostructure. ACS Energy Letters, 2018, 3, 932-939.	8.8	122
16	Potassium associated manganese vacancy in birnessite-type manganese dioxide for airborne formaldehyde oxidation. Catalysis Science and Technology, 2018, 8, 1799-1812.	2.1	117
17	Au Nanorod Photosensitized La ₂ Ti ₂ O ₇ Nanosteps: Successive Surface Heterojunctions Boosting Visible to Near-Infrared Photocatalytic H ₂ Evolution. ACS Catalysis, 2018, 8, 122-131.	5.5	114
18	Two types of cooperative nitrogen vacancies in polymeric carbon nitride for efficient solar-driven H2O2 evolution. Applied Catalysis B: Environmental, 2020, 265, 118581.	10.8	113

#	Article	IF	CITATIONS
19	Luminescent properties of a new long afterglow Eu2+ and Dy3+ activated Ca3MgSi2O8 phosphor. Journal of the European Ceramic Society, 2001, 21, 683-685.	2.8	111
20	Preparation and effects of Mg-doping on the electrochemical properties of spinel Li4Ti5O12 as anode material for lithium ion battery. Materials Chemistry and Physics, 2010, 123, 510-515.	2.0	109
21	Graphitic-C3N4 hybridized N-doped La2Ti2O7 two-dimensional layered composites as efficient visible-light-driven photocatalyst. Applied Catalysis B: Environmental, 2017, 202, 191-198.	10.8	107
22	Black phosphorus-CdS-La2Ti2O7 ternary composite: Effective noble metal-free photocatalyst for full solar spectrum activated H2 production. Applied Catalysis B: Environmental, 2019, 242, 441-448.	10.8	105
23	CuS nanoagents for photodynamic and photothermal therapies: Phenomena and possible mechanisms. Photodiagnosis and Photodynamic Therapy, 2017, 19, 5-14.	1.3	104
24	Lateral 2D WSe ₂ p–n Homojunction Formed by Efficient Chargeâ€Carrierâ€Type Modulation for Highâ€Performance Optoelectronics. Advanced Materials, 2020, 32, e1906499.	11.1	103
25	Cu2O thin films deposited by reactive direct current magnetron sputtering. Thin Solid Films, 2009, 517, 5700-5704.	0.8	102
26	Enhanced stability of black phosphorus field-effect transistors with SiO ₂ passivation. Nanotechnology, 2015, 26, 435702.	1.3	102
27	Luminescent Properties of the BaMgAl10O17:Eu2+,M3+(M = Nd, Er) Phosphor in the VUV Region. Chemistry of Materials, 2002, 14, 3005-3008.	3.2	98
28	Nitric acid-treated birnessite-type MnO2: An efficient and hydrophobic material for humid ozone decomposition. Applied Surface Science, 2018, 442, 640-649.	3.1	98
29	Reversible 3D optical data storage and information encryption in photo-modulated transparent glass medium. Light: Science and Applications, 2021, 10, 140.	7.7	95
30	TiO ₂ Film/Cu ₂ O Microgrid Heterojunction with Photocatalytic Activity under Solar Light Irradiation. ACS Applied Materials & amp; Interfaces, 2009, 1, 2111-2114.	4.0	94
31	A New Modality for Cancer Treatment—Nanoparticle Mediated Microwave Induced Photodynamic Therapy. Journal of Biomedical Nanotechnology, 2016, 12, 1835-1851.	0.5	94
32	High-Efficiency Violet-Emitting All-Inorganic Perovskite Nanocrystals Enabled by Alkaline-Earth Metal Passivation. Chemistry of Materials, 2019, 31, 3974-3983.	3.2	90
33	Morphology-controlled hydrothermal synthesis and growth mechanism of microcrystal Cu2O. CrystEngComm, 2011, 13, 633-636.	1.3	81
34	Microsized BiOCl Square Nanosheets as Ultraviolet Photodetectors and Photocatalysts. ACS Applied Materials & Interfaces, 2016, 8, 6662-6668.	4.0	81
35	Insights into the local structure of dopants, doping efficiency, and luminescence properties of lanthanide-doped CsPbCl ₃ perovskite nanocrystals. Journal of Materials Chemistry C, 2019, 7, 3037-3048.	2.7	79
36	Inert basal plane activation of two-dimensional ZnIn ₂ S ₄ <i>via</i> Ni atom doping for enhanced co-catalyst free photocatalytic hydrogen evolution. Journal of Materials Chemistry A, 2020, 8, 13376-13384.	5.2	79

#	Article	IF	CITATIONS
37	Exploration of Graphitic-C ₃ N ₄ Quantum Dots for Microwave-Induced Photodynamic Therapy. ACS Biomaterials Science and Engineering, 2017, 3, 1836-1844.	2.6	78
38	Concentrating electron and activating H-OH bond of absorbed water on metallic NiCo2S4 boosting photocatalytic hydrogen evolution. Nano Energy, 2022, 95, 107028.	8.2	78
39	Crystal structure and optical properties of white light-emitting Y2WO6:Sm3+ phosphor with excellent color rendering. RSC Advances, 2013, 3, 9029.	1.7	76
40	First-principles calculation of compensated (2N, W) codoping impacts on band gap engineering in anatase TiO2. Chemical Physics Letters, 2012, 527, 63-66.	1.2	75
41	Fabrication of vertical orthorhombic/hexagonal tungsten oxide phase junction with high photocatalytic performance. Applied Catalysis B: Environmental, 2017, 207, 207-217.	10.8	73
42	Facile synthesis of Fe-modified manganese oxide with high content of oxygen vacancies for efficient airborne ozone destruction. Applied Catalysis A: General, 2017, 546, 79-86.	2.2	69
43	Resonant Raman scattering and photoluminescence from high-quality nanocrystalline ZnO thin films prepared by thermal oxidation of ZnS thin films. Journal Physics D: Applied Physics, 2001, 34, 3430-3433.	1.3	68
44	Synthesis of nanosized rutile TiO2 powder at low temperature. Materials Chemistry and Physics, 2003, 77, 314-317.	2.0	68
45	Rapid Fabrication of Large-Area Colloidal Crystal Monolayers by a Vortical Surface Method. Langmuir, 2006, 22, 7101-7104.	1.6	63
46	Two-photon induced NIR active core-shell structured WO3/CdS for enhanced solar light photocatalytic performance. Applied Catalysis B: Environmental, 2020, 272, 118979.	10.8	62
47	Melem: an efficient metal-free luminescent material. Journal of Materials Chemistry C, 2017, 5, 10746-10753.	2.7	61
48	Optical simulation and preparation of novel Mo/ZrSiN/ZrSiON/SiO 2 solar selective absorbing coating. Solar Energy Materials and Solar Cells, 2017, 167, 178-183.	3.0	59
49	Highly efficient hydrogen production and formaldehyde degradation by Cu2O microcrystals. Applied Catalysis B: Environmental, 2015, 172-173, 1-6.	10.8	58
50	Visible-light-driven water splitting by yolk-shelled ZnIn2S4-based heterostructure without noble-metal co-catalyst and sacrificial agent. Applied Catalysis B: Environmental, 2021, 297, 120391.	10.8	58
51	Preparation and characterization of a new long afterglow indigo phosphor Ca12Al14O33:Nd,Eu. Materials Letters, 2003, 57, 4315-4318.	1.3	57
52	Photocatalytic degradation of methylene blue by ZnGa2O4 thin films. Catalysis Communications, 2009, 10, 1781-1785.	1.6	57
53	Biexciton Formation in Bilayer Tungsten Disulfide. ACS Nano, 2016, 10, 2176-2183.	7.3	57
54	Luminescent properties of Y2O3:Eu synthesized by sol–gel processing. Journal of Materials Processing Technology, 2002, 121, 265-268.	3.1	54

#	Article	IF	CITATIONS
55	Photocatalytic hydrogen generation enhanced by band gap narrowing and improved charge carrier mobility in AgTaO3 by compensated co-doping. Physical Chemistry Chemical Physics, 2013, 15, 16220.	1.3	54
56	Structural, optical and photoluminescence properties of Ga2O3 thin films deposited by vacuum thermal evaporation. Journal of Luminescence, 2019, 206, 53-58.	1.5	53
57	Spectrum designation and effect of Al substitution on the luminescence of Cr3+ doped ZnGa2O4 nano-sized phosphors. Journal of Luminescence, 2010, 130, 1738-1743.	1.5	52
58	Essential role of oxygen vacancy in electrochromic performance and stability for WO3-y films induced by atmosphere annealing. Electrochimica Acta, 2020, 332, 135504.	2.6	52
59	Au/La ₂ Ti ₂ O ₇ Nanostructures Sensitized with Black Phosphorus for Plasmonâ€Enhanced Photocatalytic Hydrogen Production in Visible and Nearâ€Infrared Light. Angewandte Chemie, 2017, 129, 2096-2100.	1.6	51
60	Two-dimensional TiO2-g-C3N4 with both Ti N and C O bridges with excellent conductivity for synergistic photoelectrocatalytic degradation of bisphenol A. Journal of Colloid and Interface Science, 2019, 557, 227-235.	5.0	51
61	Exploration of TiO2 nanoparticle mediated microdynamic therapy on cancer treatment. Nanomedicine: Nanotechnology, Biology, and Medicine, 2019, 18, 272-281.	1.7	51
62	Synthesis of nanometer Y2O3:Eu phosphor and its luminescence property. Materials Science & Engineering A: Structural Materials: Properties, Microstructure and Processing, 2002, 334, 246-249.	2.6	49
63	Antithermal Quenching of Luminescence in Zero-Dimensional Hybrid Metal Halide Solids. Journal of Physical Chemistry Letters, 2020, 11, 2902-2909.	2.1	49
64	A Nonâ€rareâ€Earth Ions Selfâ€Activated White Emitting Phosphor under Single Excitation. Advanced Functional Materials, 2015, 25, 6833-6838.	7.8	48
65	W ⁵⁺ –W ⁵⁺ Pair Induced LSPR of W ₁₈ O ₄₉ to Sensitize ZnIn ₂ S ₄ for Fullâ€Spectrum Solarâ€Lightâ€Driven Photocatalytic Hydrogen Evolution. Advanced Functional Materials, 2022, 32, .	7.8	48
66	Tuning oxygen vacancy photoluminescence in monoclinic Y2WO6 by selectively occupying yttrium sites using lanthanum. Scientific Reports, 2015, 5, 9443.	1.6	46
67	Oxygen Vacancy Effect on Photoluminescence Properties of Self-Activated Yttrium Tungstate. Journal of Physical Chemistry C, 2014, 118, 25633-25642.	1.5	45
68	Enhancing blue luminescence from Ce-doped ZnO nanophosphor by Li doping. Nanoscale Research Letters, 2014, 9, 480.	3.1	44
69	High performance in electrochromic amorphous WOx film with long-term stability and tunable switching times via Al/Li-ions intercalation/deintercalation. Electrochimica Acta, 2019, 318, 644-650.	2.6	43
70	Photocatalytic performance of ZnGa2O4 for degradation of methylene blue and its improvement by doping with Cd. Catalysis Communications, 2010, 11, 1104-1108.	1.6	42
71	Red luminescent and structural properties of Mg-doped ZnO phosphors prepared by sol–gel method. Materials Science and Engineering B: Solid-State Materials for Advanced Technology, 2012, 177, 689-693.	1.7	41
72	Spin pumping during the antiferromagnetic–ferromagnetic phase transition of iron–rhodium. Nature Communications, 2020, 11, 275.	5.8	41

#	Article	IF	CITATIONS
73	Doping indium in β-Bi ₂ O ₃ to tune the electronic structure and improve the photocatalytic activities: first-principles calculations and experimental investigation. Physical Chemistry Chemical Physics, 2014, 16, 23476-23482.	1.3	40
74	Exposed facet and crystal phase tuning of hierarchical tungsten oxide nanostructures and their enhanced visible-light-driven photocatalytic performance. CrystEngComm, 2015, 17, 9102-9110.	1.3	40
75	Reduced graphene oxide three-dimensionally wrapped WO3 hierarchical nanostructures as high-performance solar photocatalytic materials. Applied Catalysis A: General, 2016, 522, 90-100.	2.2	40
76	Enhanced photocatalytic performance of tungsten oxide through tuning exposed facets and introducing oxygen vacancies. Journal of Alloys and Compounds, 2017, 708, 358-366.	2.8	39
77	A New Luminescent Phenomenon of ZnO Due to the Precipitate Trapping Effect of MgO. Chemistry of Materials, 2004, 16, 768-770.	3.2	38
78	pHâ€Dependent Cancerâ€Directed Photodynamic Therapy by a Waterâ€6oluble Graphiticâ€Phase Carbon Nitride–Porphyrin Nanoprobe. ChemPlusChem, 2016, 81, 535-540.	1.3	38
79	Large spin-orbit splitting in the conduction band of halogen (F, Cl, Br, and I) doped monolayer <mml:math xmlns:mml="http://www.w3.org/1998/Math/MathML"><mml:mrow><mml:mi mathvariant="normal">W<mml:msub><mml:mi mathvariant="normal">S<mml:mn>2</mml:mn></mml:mi </mml:msub></mml:mi </mml:mrow></mml:math> with	1.1	38
80	Thermal convection induced TiO ₂ microclews as superior electrode materials for lithium-ion batteries. Journal of Materials Chemistry A, 2018, 6, 11688-11693.	5.2	38
81	Band gap narrowing in nitrogen-doped La ₂ Ti ₂ O ₇ predicted by density-functional theory calculations. Physical Chemistry Chemical Physics, 2015, 17, 8994-9000.	1.3	37
82	Photocatalytic property of ZnO microrods modified by Cu2O nanocrystals. Journal of Alloys and Compounds, 2013, 552, 299-303.	2.8	35
83	Mn2+ luminescence in (Ce,Tb)MgAl11O19 phosphor. Materials Chemistry and Physics, 2001, 72, 81-84.	2.0	34
84	Light-storing photocatalyst. Applied Physics Letters, 2004, 85, 5778-5780.	1.5	34
85	Methods to improve the photocatalytic activity of immobilized ZnO/Bi2O3 composite. Applied Catalysis A: General, 2011, 402, 80-86.	2.2	34
86	Synthesis and conjugation of Sr2MgSi2O7:Eu2+, Dy3+ water soluble afterglow nanoparticles for photodynamic activation. Photodiagnosis and Photodynamic Therapy, 2016, 16, 90-99.	1.3	34
87	Charge separation in a nanostep structured perovskite-type photocatalyst induced by successive surface heterojunctions. Journal of Materials Chemistry A, 2017, 5, 10442-10449.	5.2	34
88	Evaluating the electric property of different crystal faces and enhancing the Raman scattering of Cu2O microcrystal by depositing Ag on the surface. Current Applied Physics, 2013, 13, 935-939.	1.1	33
89	Two dimensional perovskite La 2 Ti 2 O 7 nanosheet as Pt catalyst support for photo-assisted methanol oxidation reaction. Journal of the Taiwan Institute of Chemical Engineers, 2017, 80, 231-238.	2.7	32
90	Preparation and optical properties of ZnGa2O4:Cr3+ thin films derived by sol–gel process. Applied Surface Science, 2010, 256, 4702-4707.	3.1	31

#	Article	IF	CITATIONS
91	Spintronic materials and devices based on antiferromagnetic metals. Progress in Natural Science: Materials International, 2017, 27, 208-216.	1.8	31
92	Role of Halogen Atoms on High-Efficiency Mn ²⁺ Emission in Two-Dimensional Hybrid Perovskites. Journal of Physical Chemistry Letters, 2019, 10, 4706-4712.	2.1	31
93	Synthesis and photoluminescent properties of Eu3+-doped ZnGa2O4 nanophosphors. Materials Science and Engineering B: Solid-State Materials for Advanced Technology, 2008, 149, 82-86.	1.7	29
94	Single-phased emission-tunable Mg-doped ZnO phosphors for white LEDs. Journal of Alloys and Compounds, 2013, 553, 172-176.	2.8	29
95	Tuning Phosphorene Nanoribbon Electronic Structure through Edge Oxidization. Journal of Physical Chemistry C, 2016, 120, 2149-2158.	1.5	28
96	Luminescence and theoretical calculations of novel red-emitting NaYPO 4 F:Eu 3+ phosphor for LED applications. Journal of Alloys and Compounds, 2017, 712, 225-232.	2.8	28
97	Synthesis and characterization of BaMgAl10O17:Eu phosphors derived by sol–gel processing. Powder Technology, 2002, 126, 161-165.	2.1	27
98	A new method to synthesize long afterglow red phosphor. Ceramics International, 2004, 30, 225-228.	2.3	27
99	Highly Efficient Metal-Free Two-Dimensional Luminescent Melem Nanosheets for Bioimaging. ACS Applied Materials & Interfaces, 2020, 12, 2145-2151.	4.0	27
100	Spatial carrier separation in cobalt phosphate deposited ZnIn2S4 nanosheets for efficient photocatalytic hydrogen evolution. Journal of Colloid and Interface Science, 2022, 606, 317-327.	5.0	27
101	Band gap engineering of compensated (N, H) and (C, 2H) codoped anatase TiO2: A first-principles calculation. Chemical Physics Letters, 2012, 539-540, 175-179.	1.2	26
102	Effects of oxygen vacancies on luminescent properties of green long-lasting phosphorescent (LLP) material α-Zn3(PO4)2: Mn2+, K+. Journal of Luminescence, 2016, 170, 150-154.	1.5	26
103	Effect of Dy ³⁺ and Eu ³⁺ 4f Band Gap States on Luminescence and Energy Transfer in Monoclinic Lutetium Tungstate. ACS Applied Electronic Materials, 2019, 1, 772-782.	2.0	26
104	Unraveling the mechanochemical synthesis and luminescence in MnII-based two-dimensional hybrid perovskite (C4H9NH3)2PbCl4. Science China Materials, 2019, 62, 1013-1022.	3.5	26
105	Synthesis of large-sized monodisperse polystyrene microspheres by dispersion polymerization with dropwise monomer feeding procedure. Colloid and Polymer Science, 2009, 287, 243-248.	1.0	24
106	Synthesis, Characterization and Photocatalytic Activity of TiO2 Film/Bi2O3 Microgrid Heterojunction. Journal of Materials Science and Technology, 2011, 27, 59-63.	5.6	24
107	Electronic structure and photocatalytic activity of N/Mo doped anatase TiO2. Catalysis Communications, 2012, 29, 175-179.	1.6	24
108	Defects enhanced photoluminescence of Mn2+-doped ZrP2O7 blue LLP materials. Journal of Alloys and Compounds, 2019, 789, 375-380.	2.8	24

#	Article	IF	CITATIONS
109	Activating MoS ₂ basal planes for hydrogen evolution through direct CVD morphology control. Journal of Materials Chemistry A, 2019, 7, 27603-27611.	5.2	24
110	X-ray excited luminescence and persistent luminescence of Sr2MgSi2O7:Eu2+, Dy3+ and their associations with synthesis conditions. Journal of Luminescence, 2018, 198, 132-137.	1.5	23
111	Preparation of 0D/2D ZnFe2O4/Fe-doped g-C3N4 hybrid photocatalysts for visible light N2 fixation. Journal of Alloys and Compounds, 2021, 869, 158809.	2.8	23
112	Influence of Metal (Au, Ag) Micro-Grid on the Photocatalytic Activity of TiO2 Film. Catalysis Letters, 2008, 123, 51-55.	1.4	22
113	Effects of atomic oxygen treatment on structures, morphologies and electrical properties of ZnO:Al films. Applied Surface Science, 2010, 256, 4527-4532.	3.1	22
114	Hierarchical-structure anatase TiO2 with conductive network for high-rate and high-loading lithium-ion battery. Science Bulletin, 2019, 64, 1148-1151.	4.3	22
115	Luminescence of Cr3+-doped ZnGa2O4 thin films deposited by pulsed laser ablation. Thin Solid Films, 2012, 520, 6845-6849.	0.8	21
116	Phosphorescence behavior and photoluminescence mechanism of Dy 3+ sensitized β-Zn 3 (PO 4) 2 : Mn 2+ phosphor. Journal of Alloys and Compounds, 2015, 642, 225-231.	2.8	21
117	Giant Enhancement of Luminescence from Phosphors through Oxygenâ€Vacancyâ€Mediated Chemical Pressure Relaxation. Advanced Optical Materials, 2017, 5, 1700448.	3.6	21
118	A newly designed porous oxynitride photoanode with enhanced charge carrier mobility. Nano Energy, 2017, 39, 172-182.	8.2	21
119	Preparation and properties of photoluminescent rare earth doped SrO–MgO–B2O3–SiO2 glass. Materials Science and Engineering B: Solid-State Materials for Advanced Technology, 2001, 86, 79-82.	1.7	20
120	Blue-emitting ZnO sol and film obtained by sol-gel process. Journal of Sol-Gel Science and Technology, 2006, 39, 37-39.	1.1	20
121	PL and EL characterizations of ZnO:Eu3+, Li+ films derived by sol–gel process. Journal of Luminescence, 2008, 128, 685-689.	1.5	20
122	Density functional theory calculations of surface properties and H2 adsorption on the Cu2O (111) surface. Applied Surface Science, 2011, 257, 10710-10714.	3.1	20
123	Mn doped hard type perovskite high-temperature BYPT–PZN ternary piezoelectric ceramics. Sensors and Actuators A: Physical, 2014, 216, 335-341.	2.0	20
124	Epitaxial Templating of Two-Dimensional Metal Chloride Nanocrystals on Monolayer Molybdenum Disulfide. ACS Nano, 2017, 11, 6404-6415.	7.3	20
125	Theoryâ€Guided Defect Tuning through Topochemical Reactions for Accelerated Discovery of UVC Persistent Phosphors. Advanced Optical Materials, 2020, 8, 1901727.	3.6	20
126	Enhanced Stability of Black Phosphorus Fieldâ€Effect Transistors via Hydrogen Treatment. Advanced Electronic Materials, 2018, 4, 1700455.	2.6	19

#	Article	IF	CITATIONS
127	Advances in anti-relaxation coatings of alkali-metal vapor cells. Applied Surface Science, 2020, 501, 143897.	3.1	19
128	Enhanced photocatalytic activity of Ag microgrid connected TiO2 nanocrystalline films. Applied Physics Letters, 2007, 90, 122114.	1.5	18
129	Facile access to shape-controlled growth of WS ₂ monolayer via environment-friendly method. 2D Materials, 2019, 6, 015007.	2.0	18
130	Luminescent properties of ZnO sol and film doped with Tb3+ ion. Materials Science & Engineering A: Structural Materials: Properties, Microstructure and Processing, 2006, 425, 346-348.	2.6	17
131	Electro-optical performance of inorganic monolithic electrochromic device with a pulsed DC sputtered Li x Mg y N ion conductor. Journal of Solid State Electrochemistry, 2018, 22, 275-283.	1.2	17
132	Enhanced properties of LiFePO4/C cathode materials modified by CePO4 nanoparticles. Materials Chemistry and Physics, 2014, 147, 333-338.	2.0	16
133	Investigating the interlayer electron transport and its influence on the whole electric properties of black phosphorus. Science Bulletin, 2019, 64, 254-260.	4.3	16
134	Tackling Challenges in Perovskiteâ€īype Metal Oxide Photocatalysts. Energy Technology, 2021, 9, 2001019.	1.8	16
135	Effects of Bi-dopant and co-catalysts upon hole surface trapping on La2Ti2O7 nanosheet photocatalysts in overall solar water splitting. Nano Research, 2022, 15, 438-445.	5.8	16
136	Effect of MgO doping on the luminescent properties of ZnO. Materials Science and Engineering B: Solid-State Materials for Advanced Technology, 2006, 129, 93-95.	1.7	15
137	Luminescence of nanosized ZnO/polyaniline films prepared by self-assembly. Ceramics International, 2007, 33, 785-788.	2.3	15
138	Oxygen vacancy in N-doped Cu ₂ O crystals: A density functional theory study. Chinese Physics B, 2012, 21, 087301.	0.7	15
139	Structure and electrical properties of (1â^' x)(0.1BiYbO 3 –0.9PbTiO 3)– x Pb(Zn 1/3 Nb 2/3)O 3 high-temperature ternary piezoelectric ceramics. Materials Letters, 2014, 114, 100-102.	1.3	15
140	Phosphorescence properties and energy transfer of red long-lasting phosphorescent (LLP) material β-Zn3(PO4)2:Mn2+,Pr3+. Journal of Rare Earths, 2015, 33, 1056-1063.	2.5	15
141	Hydrogen atom etching induced large-size ultrathin g-C3N4 nanosheets for enhanced photoluminescence. Journal of Luminescence, 2019, 206, 660-665.	1.5	14
142	Yb ³⁺ Doping Monoclinic Lu ₂ WO ₆ : Near-Infrared Emission and Energy-Transfer Luminescence Mechanism. Journal of Physical Chemistry C, 2018, 122, 21607-21616.	1.5	13
143	Coarse-grained reduced Mo Ti1â^'Nb2O7+ anodes for high-rate lithium-ion batteries. Energy Storage Materials, 2021, 34, 574-581.	9.5	13
144	Photocatalytic H2 evolution over sulfur vacancy-rich ZnIn2S4 hierarchical microspheres under visible light. Journal of Materials Science, 2021, 56, 19439-19451.	1.7	13

#	Article	IF	CITATIONS
145	Semiconductor heterojunction photocatalysts with near-infrared light antennas: a review. Journal Physics D: Applied Physics, 2021, 54, 313002.	1.3	12
146	High efficiency degradation of tetracycline and rhodamine B using Z-type BaTiO3/γ-Bi2O3 heterojunction. Separation and Purification Technology, 2021, 278, 119666.	3.9	12
147	Enhanced fluorescence from Mg0.1Zn0.9O due to localized surface plasmon resonance of Ag nanoparticles. Materials and Design, 2016, 110, 138-144.	3.3	11
148	Luminescent properties of (Ce0.67Tb0.33)MnxMg1â^'xAl11O19 phosphor in VUV region. Ceramics International, 2003, 29, 583-586.	2.3	10
149	A density functional theory study on the adsorption of CO and O 2 on Cu-terminated Cu 2 O (111) surface. Chinese Physics B, 2012, 21, 067302.	0.7	10
150	Preparation and properties of tungsten-doped indium oxide thin films. Rare Metals, 2012, 31, 158-163.	3.6	10
151	One-step synthesis of high photocatalytic graphitic carbon nitride porous nanosheets. Nanotechnology, 2020, 31, 464001.	1.3	10
152	Enhancing Photocatalytic Hydrogen Production of g-C3N4 by Selective Deposition of Pt Cocatalyst. Nanomaterials, 2021, 11, 3266.	1.9	10
153	Sunlight driven isotropic β-Bi ₂ O ₃ with high charge-carrier mobility for the efficient degradation of bisphenol A and phenol. Dalton Transactions, 2022, 51, 8401-8410.	1.6	10
154	Effect of Gap Filler on Microstructure of Wide Gap Brazing Seam. Materials Transactions, JIM, 2000, 41, 1073-1076.	0.9	9
155	Green-emission and n-type conductivity of ZnO:Zn films obtained using vapor deposition method. Applied Surface Science, 2009, 255, 3530-3533.	3.1	9
156	Time-dependent hydrothermal synthesis and self-evolution mechanism of Cu2O microcrystals. Materials Characterization, 2012, 71, 112-119.	1.9	9
157	Dependence of Luminescence Efficiency of CdSe Quantum Dots on Chemical Environments. Journal of Nanoscience and Nanotechnology, 2008, 8, 5615-5623.	0.9	8
158	Controllable growth and photocatalytic activity of Cu2O solid microspheres. Materials Research Bulletin, 2013, 48, 3431-3437.	2.7	8
159	Role of an ultrathin platinum seed layer in antiferromagnet-based perpendicular exchange coupling and its electrical manipulation. Journal of Magnetism and Magnetic Materials, 2017, 428, 431-436.	1.0	8
160	Insitu growth of BiVO4/HoVO4 heterojunction with O O bond connection for enhanced photodegradation activity. Materials Letters, 2021, 284, 128952.	1.3	8
161	Excitonic photoluminescence characteristics of amorphous silicon nanoparticles embedded in silicon nitride film. European Physical Journal B, 2007, 57, 53-56.	0.6	7
162	Effects of dopant content on optical and electrical properties of In2O3: W transparent conductive films. Rare Metals, 2012, 31, 168-171.	3.6	7

#	Article	IF	CITATIONS
163	Microsphere morphology tuning and photo-luminescence properties of monoclinic Y2WO6. Journal of Crystal Growth, 2015, 416, 148-153.	0.7	7
164	Theoretical studies on the energy structures and optical properties of copper cysteamine – a novel sensitizer. Physical Chemistry Chemical Physics, 2019, 21, 21084-21093.	1.3	7
165	Photogenerated charge separation and recombination path modification in monocline Lu2WO6via lattice transition and Bi–O antibonding states. Dalton Transactions, 2021, 50, 6659-6666.	1.6	7
166	Formation of Cu0 in Cu2O under light irradiation and subsequent accelerated decoloration to MO aqueous solution. Catalysis Communications, 2011, 16, 175-179.	1.6	6
167	Effect of Cu ₂ O Morphology on Photocatalytic Hydrogen Generation and Chemical Stability of TiO ₂ /Cu ₂ O Composite. Journal of Nanoscience and Nanotechnology, 2013, 13, 5104-5108.	0.9	6
168	Achieving giant spin-orbit splitting in conduction band of monolayer WS2 via n-p co-doping. AIP Advances, 2019, 9, 075304.	0.6	6
169	Microwave-initiated recombination of hydrogen bonds of a perylene diimide supramolecule for PPCP photodegradation. Catalysis Science and Technology, 2021, 11, 3787-3798.	2.1	6
170	van der Waals g-C ₃ N ₄ /BiLuWO ₆ Heterojunctions from Theoretical Predictions to Photocatalytic Applications. Journal of Physical Chemistry C, 2021, 125, 19763-19772.	1.5	6
171	Synthesis and Characterization of (Ce _{0.67} Tb _{0.33})Mn _{<i>x</i>} Mg _{1â~°<i>x</i>} Al _{11Phosphors Derived by Sol–Gel Processing. Journal of the American Ceramic Society, 2002, 85, 998-1000.}	>O ts ub>1	9<ѣub>
172	Silver microgrid transparent conductive electrode based on bulk plasmon effect for ultraviolet wavelength application. Physica Status Solidi - Rapid Research Letters, 2013, 7, 1071-1075.	1.2	5
173	Electronic structures of anatase (TiO ₂) _{1â^'x} (TaON) _x solid solutions: a first-principles study. Physical Chemistry Chemical Physics, 2015, 17, 17980-17988.	1.3	5
174	Skin formation in drying a film of soft matter solutions: Application of solute based Lagrangian scheme. Chinese Physics B, 2016, 25, 076801.	0.7	5
175	Investigation of luminescence mechanism in La0.2Y1.8O3 scintillator. Journal of Luminescence, 2016, 173, 99-104.	1.5	5
176	Realization of valley polarization in monolayer WS ₂ via 3 <i>d</i> transition metal atom adsorption. Journal Physics D: Applied Physics, 2020, 53, 384001.	1.3	5
177	Photocatalytic activity of ZnO films with micro-grid structure. Frontiers of Environmental Science and Engineering in China, 2009, 3, 289-293.	0.8	4
178	Defective [Bi ₂ O ₂] ²⁺ Layers Exhibiting Ultrabroad Nearâ€Infrared Luminescence. Chemistry - A European Journal, 2019, 25, 12842-12848.	1.7	4
179	Boosting the photocatalytic H ₂ evolution activity of a CdS/N-doped ZnIn ₂ S ₄ direct Z-scheme heterostructure using a band alignment regulation strategy. Sustainable Energy and Fuels, 2021, 5, 6441-6448.	2.5	4
180	Photocatalytic performance of TiO2 thin films connected with Cu micro-grid. Science in China Series D: Earth Sciences, 2009, 52, 2175-2179.	0.9	3

#	Article	IF	CITATIONS
181	Employment of a metal microgrid as a front electrode in a sandwich-structured photodetector. Applied Optics, 2009, 48, 3638.	2.1	3
182	White Light Phosphors: A Nonrare-Earth Ions Self-Activated White Emitting Phosphor under Single Excitation (Adv. Funct. Mater. 44/2015). Advanced Functional Materials, 2015, 25, 6826-6826.	7.8	3
183	Facile synthesis of CTAB assisted hierarchical-structure TiO2@SnO2 for lithium storage. Solid State Sciences, 2020, 100, 106114.	1.5	3
184	Construction of a 3D/2D plasmonic Z-scheme heterojunction with electrostatic self-assembly for full-spectrum solar-light driven photocatalytic protons reduction. Materials Today Advances, 2022, 15, 100249.	2.5	3
185	Catalyst-free growth of green-emitting arrayed ZnO nanorods at low temperature. Materials Science and Engineering B: Solid-State Materials for Advanced Technology, 2008, 151, 187-190.	1.7	2
186	Fabrication and luminescent properties of artificial luminous gem. Ceramics International, 2010, 36, 1201-1203.	2.3	2
187	LUMINESCENT PROPERTY OF ZNO GRANULAR FILMS WITH DIFFERENT PARTICLE SIZE. International Journal of Modern Physics B, 2010, 24, 2827-2832.	1.0	2
188	Highâ€Performance Optoelectronics: Lateral 2D WSe ₂ p–n Homojunction Formed by Efficient Chargeâ€Carrierâ€Type Modulation for Highâ€Performance Optoelectronics (Adv. Mater. 9/2020). Advanced Materials, 2020, 32, 2070067.	11.1	2
189	First-Principles Calculation of Luminescent Materials. , 2017, , 173-218.		1
190	Transformation of Perovskite BaBiO ₃ into Layered BaBiO _{2.5} Crystals Featuring Unusual Chemical Bonding and Luminescence. Chemistry - A European Journal, 2018, 24, 8875-8882.	1.7	1
191	High-loaded and transparent La _{<i>x</i>} Ce ₁₋ _{<i>x</i>} F ₃ — polystyrene nanocomposite scintillators for radiation detection. Canadian Journal of Chemistry, 2017, 95, 1233-1240.	0.6	0
192	Lateral p-n Homojunction formed by Local Doping for High-Performance Photodetector. , 2021, , .		0
193	EFFECT OF AMBIENT RELATIVE HUMIDITY AND SOAKING TIME ON THE FORMATION OF OCTADECYLTRICHLOROSILANE COATINGS ON BOROSILICATE GLASS SUBSTRATES FOR ALKALI-METAL VAPOR CELLS. Surface Review and Letters, 0, , .	0.5	0